**Journal of Nuclear Medicine, published on May 21, 2015 as doi:10.2967/jnumed.114.149690**



# $^{89}$Zr- *versus* $^{124}$I-labeled αHER2 Fab with optimized plasma-half life for high contrast tumor imaging in vivo

Claudia T. Mendler[1,2], Torben Gehring[1], Hans-Jürgen Wester[3], Markus Schwaiger[2], Arne Skerra[1*]

[1] Munich Center for Integrated Protein Science (CIPS-M) and Lehrstuhl für Biologische Chemie, Technische Universität München, 85350 Freising-Weihenstephan, Germany

[2] Nuklearmedizinische Klinik und Poliklinik, Klinikum rechts der Isar, Technische Universität München, 81675 München, Germany

[3] Pharmazeutische Radiochemie, Technische Universität München, 85748 Garching, Germany

*To whom correspondence should be addressed:

Prof. Dr. Arne Skerra, Lehrstuhl für Biologische Chemie, Technische Universität München, Emil-Erlenmeyer-Forum 5, 85350 Freising-Weihenstephan, Germany; phone: +49 8161 71 4351; fax: +49 8161 71 4352; e-mail: skerra@tum.de

*Running title:* $^{89}$Zr- *vs.* $^{124}$I-labeled αHER2 Fab tracer

*Word count*: 5254

**ABSTRACT**

Immuno-PET imaging of the tumor antigen HER2/neu allows for the non-invasive detection and monitoring of oncogene expression, which is of prognostic value in patients with breast cancer. Compared with the full size antibody Trastuzumab, smaller protein tracers with more rapid blood clearance permit higher imaging contrast at earlier time points. Antigen-binding fragments (Fabs) of antibodies with moderately prolonged circulation via PASylation, a convenient biological alternative to PEGylation, offer a promising tracer format with improved pharmacokinetics for in vivo imaging. The transition radiometal $^{89}$Zr has attracted increasing interest for immuno-PET studies, thus complementing the conventional halogen radionuclide $^{124}$I. **Methods.** To directly compare these two radioactive labels using the same protein tracer, the recombinant αHER2 Fab fused with 200 PAS residues was either conjugated with $^{124}$I, via the Iodogen method, or coupled with deferoxamine thiocyanate, followed by complexation of $^{89}$Zr. After confirming stability of both radioconjugates and quality control in vitro, immuno-PET and biodistribution studies were performed in CD1-*Foxn1$^{nu}$* mice bearing HER2-positive human tumor xenografts. **Results.** $^{89}$Zr•Df-Fab-PAS$_{200}$ and $^{124}$I-Fab-PAS$_{200}$ showed specific tumor uptake of 11 % ID/g and 2.3 % ID/g 24 h p.i., respectively, both with high tumor-to-blood (3.6 and 4.4) and tumor-to-muscle (20 and 43) ratios. With regard to off-target accumulation, overt $^{124}$I activity was seen in the thyroid, as expected, whereas high kidney uptake was evident for $^{89}$Zr, probably due to glomerular filtration and reabsorption of the protein tracer in proximal tubular cells. **Conclusions.** Both the $^{89}$Zr- and $^{124}$I-labeled version of αHER2 Fab-PAS$_{200}$ allow PET tumor imaging with high contrast, while the tracer $^{89}$Zr•Df-Fab-PAS$_{200}$ with its residualizing radiometal shows better in vivo stability and higher tumor uptake.

*Key words*: Fab, HER2, PASylation, plasma half-life, positron emission tomography

**INTRODUCTION**

The human epidermal growth factor receptor 2 (HER2/*neu*) is overexpressed in various cancer types and usually associated with an aggressive tumor phenotype as well as poor prognosis, which makes it an important target for cancer diagnosis and therapy (*1*). Especially immuno-PET, with its high target specificity and spatial resolution as well as the possibility for quantitative imaging (*2*), can detect even poorly accessible HER2-positive lesions and metastases (*3*), provided that a potent HER2-specific tracer is available.

Both the halogen radionuclide $^{124}$I and the transition metal radionuclide $^{89}$Zr are convenient positron emitters and have been employed for coupling to mAbs in many immuno-PET studies (*4, 5*). Radioiodinated proteins often show high imaging contrast, but they are less stable both during storage and application in vivo, also due to dehalogenation in blood plasma and tissues. Furthermore, the high positron energy of $^{124}$I and corresponding long range in tissue may reduce spatial resolution and quantification.

On the other hand, much better spatial resolution has been observed for the residualizing radionuclide $^{89}$Zr owing to its low average positron energy of 395 keV, which is comparable to $^{18}$F (*6*). The availability of carrier-free $^{89}$Zr produced via cyclotron irradiation of naturally abundant $^{89}$Y in conjunction with the convenient chelator deferoxamine (Df) has facilitated numerous studies using $^{89}$Zr-labeled mAbs (*7*). Df provides high selectivity for Zr(VI) and extraordinary thermodynamic stability with a complex formation constant >$10^{31}$ (*8*).

Indeed, the identification of HER2-positive tumor lesions was demonstrated in several studies using $^{89}$Zr- or $^{111}$In-labeled Trastuzumab in patients with metastatic breast cancer (*9, 10*). However, with regard to imaging contrast, smaller antibody fragments should be preferable over large intact mAbs with their intrinsically long circulation. Conversely, the smaller Fabs, which are

prone to kidney filtration and lack FcRn-mediated endosomal recycling, promise faster tumor penetration but suffer from a very rapid blood clearance before sufficient accumulation in the tumor can be reached.

Recently, the PASylation technology, which involves the genetic fusion of a biopharmaceutically active protein with a long conformationally disordered chain of the natural amino acids Pro, Ala and/or Ser (PAS), has been developed as a convenient biological alternative to PEGylation. PASylation offers the opportunity to easily extend the in vivo life-time of a recombinant protein in a precise manner by expanding its hydrodynamic molecular volume and, consequently, retarding renal filtration (*11*).

We have previously applied PASylation to the Trastuzumab Fab to improve its pharmacokinetic properties for PET imaging, indicating an optimal tumor to blood ratio for a PAS tag of around 200 residues (*12*). Here, we report on the comparison between $^{89}$Zr- and $^{124}$I-labeling of the recombinant αHER2 Fab-PAS$_{200}$ protein tracer for immuno-PET imaging of HER2-positive human xenograft tumors in mice.

## MATERIALS AND METHODS

### Preparation of αHER2 Fab

Recombinant protein production in *E. coli* was performed as previously described (*12*). Purity, disulfide bond formation and hydrodynamic volume were analyzed via SDS-PAGE, SEC and, finally, ESI-MS.

### In Vitro Binding Studies of αHER2 Fab

Target affinity of the Fab and its derivatives on the HER2-positive human breast adenocarcinoma cell line SK-BR-3 (*13*) was determined via cytofluorimetric titration as described

(*12*). Therefore, $10^5$ cells were incubated with 100 µl of the purified Fab (or with Trastuzumab) at appropriate dilutions and subsequently stained with a fluorescein-conjugated anti-human-kappa-light chain antibody (Invitrogen / Life Technologies, Darmstadt, Germany), followed by counting on a FACSAria Cell-Sorting system (BD Biosciences, Heidelberg, Germany).

**Radiolabeling of Fab**

A 5-fold molar excess of Deferoxamine-*p-SCN* (Macrocyclics, Dallas, TX) was dissolved in DMSO and added to a 30 µM (2 mg/ml) solution of the purified Fab in 0.1 M $NaHCO_3$ (pH 8.5), followed by incubation over night at 25 °C. Unconjugated chelator was removed by gel filtration on a PD-10 column (GE Healthcare, Freiburg, Germany) using 20 mM HEPES/NaOH pH 7.0 as eluent. Radiolabeling of the purified Df-Fab-$PAS_{200}$ was performed according to a published procedure (*14*). Typically, 3 mCi of $^{89}$Zr(IV)-oxalate (specific activity 150 MBq/nmol; IBA Molecular, VU Amsterdam, The Netherlands) dissolved in 1 M oxalic acid were mixed with 150 µl water and 50 µl 2 M $Na_2CO_3$, followed by 3 min incubation at RT. After $CO_2$ liberation, 200 µl 0.5 M HEPES/NaOH pH 7.0 and 75 µl 1 M gentisic acid/NaOH pH 7.0 as well as 9 nmol of the Fab in a volume of ~100 µl was added and the mixture was incubated for 60 min at RT. Finally, the radiolabeled Fab was separated from free $^{89}$Zr on a PD-10 column. Radiolabeling efficiency and radiochemical purity were analyzed by thin layer chromatography (TLC) on glass micro fiber chromatography paper using 20 mM Na-citrate pH 5, as mobile phase. For SDS-PAGE analysis and in vitro antigen-binding studies, Fab was also labeled with non-radioactive Zr(IV) chloride (Sigma-Aldrich, St. Louis, MO) dissolved in 1 M oxalic acid as described above.

Radio-iodination of Fab-$PAS_{200}$ was performed using the Iodogen method as described before (*12*). Generally, 0.44 nmol of the purified Fab and 37 MBq Na$^{125}$I (specific activity 74 MBq/nmol; Hartman Analytic, Braunschweig, Germany) or Na$^{124}$I (~1.1 MBq/pmol; IBA Molecular) was incubated for 15 min at RT and separated from the reagents on a PD-10 column. Radiochemical purity was analyzed by TLC using 0.9 % w/v NaCl as mobile phase. Fab labeled with non-

radioactive iodide ($Na^{127}I$) under the same conditions was used for analysis by SDS-PAGE and tested for antigen-binding activity.

In vitro stability of $^{89}$Zr•Df-Fab-$PAS_{200}$ and $^{125}$I-Fab-$PAS_{200}$ in PBS at RT was analyzed with TLC and SEC up to 3 days after radiolabeling. For analysis of the in vivo stability, blood samples from mice injected with the radiolabeled protein (see below) were collected 24 h p.i. and serum was subjected to SDS-PAGE followed by phosphorimager analysis.

**In Vivo studies**

For biodistribution analyses and PET imaging, female CD1-*Foxn1$^{nu}$* mice (Charles River Laboratories, Sulzfeld, Germany) were injected subcutaneously with 5 x $10^6$ SK-BR-3 cells, leading to tumor sizes in the range 300–800 $mm^3$. Micro-PET studies were performed by tail vein injection of 7 MBq $^{89}$Zr- or $^{124}$I-labeled Fab-$PAS_{200}$ (n=2) with a specific activity of 11 MBq/nmol and 80 MBq/nmol, respectively. Static maximum intensity projection (MIP) images were acquired under isoflurane anesthesia using an Inveon PET/CT small animal scanner (Siemens Medical Solutions, Knoxville, TN). Quantitation of appropriate PET images (n=1–2) was performed by drawing specific regions of interest (ROI) in tumor and muscle tissue using the Inveon software.

For biodistribution studies, mice (n=5–6) were injected intravenously with 0.37–0.74 MBq of each $^{89}$Zr•Df-Fab-$PAS_{200}$ and $^{125}$I-Fab-$PAS_{200}$ at the same time. After 6 h, 24 h and 48 h, blood and organs of interest were dissected and analyzed in a Wallac Wizard γ-counter (PerkinElmer, Turku, Finland).

For blocking experiments (n=5), 0.56 mg Trastuzumab from the hospital pharmacy was injected into the tail vein once 24 h before and once along with the radiolabeled Fab.

All animal experiments were approved by local authorities (Regierung von Oberbayern, license no. 55.2-1-54-2532-46-12) and were in compliance with the regulatory and institutional guidelines.

## RESULTS

### Preparation of αHER2 Fab-PAS$_{200}$

For in vivo imaging of HER2-positive tumors, we applied the recombinant αHER2 Fab hu4D5v8 carrying a PAS-tag of 200 residues at the C-terminus of the light chain in order to achieve moderately extended plasma half-life (*11, 12*). The Fab was produced as a functional protein via periplasmic secretion in *E. coli* and purified in a functional state, including quantitative disulfide bridge formation between light and heavy chains, as confirmed by SDS-PAGE analysis (Fig. 1). Furthermore, SEC revealed a homogeneous peak with decreased elution volume, indicating an expanded molecular size of the PASylated Fab as intended.

To allow radiolabeling with $^{89}$Zr(IV), the recombinant Fab was functionalized with the chelator reagent deferoxamine thiocyanate (Df-SCN) via Lys side chains, and ESI-MS measurements revealed a chelator-to-Fab ratio of ~2:1. The biochemical integrity of the Fab after conjugation was confirmed by SDS-PAGE and SEC (data not shown). Binding activity of αHER2 Fab-PAS$_{200}$ was verified by FACS titration analysis of the HER2-positive human tumor cell line SK-BR-3 (*13*). A dissociation constant ($K_D$) of 2.2 nM was measured for the unmodified recombinant Fab, which is comparable to the $K_D$ of 1 nM determined for the parental antibody Trastuzumab (data not shown). Generally, only moderate influence on target affinity was seen in this assay by either PASylation, Zr•Df conjugation or iodination: 4.7 nM for Fab-PAS$_{200}$, 9.6 nM for $^{nat}$Zr•Df-Fab-PAS$_{200}$, and 1.8 nM for $^{127}$I-Fab (Fig. 1B).

### Radio-Isotope Labeling

For in vivo PET imaging, αHER2 Fab-PAS$_{200}$ was separately radiolabeled with each of the positron emitters $^{89}$Zr (via Df coupling) and $^{124}$I (by Iodogen labeling). For biodistribution experiments, $^{89}$Zr- and $^{125}$I-labeled proteins were applied in combination (dual tracer analysis).

Radiolabeling of Df-Fab-PAS$_{200}$ with $^{89}$Zr(IV)-oxalic acid (*14*) resulted in a reaction yield of 90–95 % after 10 min incubation at room temperature (RT), while for iodination via the Iodogen method a reaction yield of 80 % was obtained after 15 min incubation at RT. With both isotopes, radiochemical purity >98 % was determined by radio thin layer chromatography after purification on a desalting column. Tracer stability was further confirmed by SDS-PAGE analysis of the $^{89}$Zr-labeled (Fig. 1C) and iodinated Fabs (data not shown).

In vitro stability of $^{89}$Zr•Df-Fab-PAS$_{200}$ (1.5 mCi/ml) was investigated via SEC by incubation in phosphate-buffered saline (PBS) at RT, indicating that after 24 h only 2.2 %, and after 72 h 8.9 %, of the bound $^{89}$Zr was dissociated from the Fab (Fig. 1D). Similarly high tracer stability of this radiometal chelate was described in other publications (*15*). In addition, tracer stability in vivo was assessed by analyzing serum of CD1-*Foxn1$^{nu}$* mice collected 24 h post injection (p.i.) of $^{89}$Zr•Df-Fab-PAS$_{200}$ (see below). No signs of tracer degradation or loss of $^{89}$Zr•Df were observed, and an intact disulfide bridge connecting heavy and light chains was verified (Fig. 1E).

**In Vivo PET Tumor Imaging**

$^{89}$Zr- and $^{124}$I-labeled αHER2 Fab with enhanced plasma half-life were compared for in vivo PET imaging in CD1-*Foxn1$^{nu}$* mice bearing subcutaneous HER2-positive human tumor xenografts. Static maximum intensity projection (MIP) PET images were collected at appropriate time points after tracer injection (Fig. 2). Tracer specificity was confirmed in blocking experiments with an excess of unlabeled Trastuzumab. For both PASylated αHER2 Fab tracers optimal imaging contrast was already observed 24 h p.i., with high tumor-to-normal tissue contrast and stable tumor uptake up to several days.

However, despite similar tumor staining, notable differences became apparent in the metabolization of the $^{89}$Zr- and $^{124}$I-labeled protein tracers. The $^{89}$Zr-labeled Fab revealed high

kidney uptake, most likely due to renal filtration of the tracer followed by reabsorption in proximal tubular cells (*16*). Whereas $^{124}$I-Fab-PAS$_{200}$ probably gets excreted in the same way, its degradation product iodotyrosine, which becomes liberated after internalization and lysosomal degradation, is not trapped in this tissue. Instead, the iodide that is formed by dehalogenation accumulates in the thyroid by means of the sodium iodide symporter (NIS) (*17*). Furthermore, iodide is also released from blood into the acid gastric lumen as indicated in the case of $^{124}$I-Fab-PAS$_{200}$ by enhanced radioactivity in the stomach (Fig. 2).

**Biodistribution Studies**

The in vivo imaging data were complemented by dual-tracer biodistribution experiments of the PASylated αHER2 Fab, either labeled with $^{89}$Zr ($\beta^+/\gamma$) or with the iodine isotope $^{125}$I ($\gamma$), which were injected simultaneously to avoid variation in tracer administration between different animals. $^{89}$Zr•Df-Fab-PAS$_{200}$ showed high tumor accumulation with a maximum of 11 % ID/g as well as favorable tumor-to-organ ratios 24 h p.i. (Fig. 3). Lower tracer uptake compared to activity in blood was observed in all analyzed organs with exception of the kidney (88 % ID/g) and adrenal gland, as well as liver (3,7 % ID/g) and also spleen at later time points (48 h p.i.). The fast metabolism of mice is most likely responsible for degradation and/or demetalation of $^{89}$Zr•Df-Fab-PAS$_{200}$ in the liver (*18*). Interestingly, no overt accumulation in bones was detected here as it was previously observed with $^{89}$Zr•Df-Trastuzumab in mice (*19, 20*).

If labeled with $^{125}$I, Fab-PAS$_{200}$ also showed prominent tumor accumulation with a maximum of 2.3 % ID/g 24 h p.i., revealing a high tumor-to-blood ratio of 4.4 and high tumor-to-normal tissue ratios (Table 1). With exception of the thyroid, almost no unspecific tracer uptake was seen in any other analyzed organ (Fig. 3B), probably due to the non-residualizing character of this radioisotope. Finally, tracer specificity was verified with blocking experiments by injection of a

1000-fold molar excess of Trastuzumab, which resulted in a 3.3-fold ($^{89}$Zr•Df-Fab-PAS$_{200}$) and 6.3-fold ($^{125}$I-Fab-PAS$_{200}$) reduction in tumor uptake ($p < 0.001$) 24 h p.i., respectively (Table 1).

Remarkably, when comparing the two radioisotopes, the $^{89}$Zr-labeled Fab showed 4.8-fold higher total tumor uptake 24 h p.i. than the $^{125}$I-labeled Fab, whereas similar tumor-to-blood ratios were observed with both labels (Fig. 3C). This is in line with the residualizing nature of this radiometal, which stays trapped inside tumor cells after receptor-mediated endocytosis and lysosomal tracer degradation (*21, 22*). Notably, however, the two tracers showed differing unspecific accumulation, either in thyroid ($^{125}$I) or in the kidney ($^{89}$Zr), thus leading to high organ-to-tumor ratios there.

The biodistribution data were essentially in accordance with the PET experiments, where similar uptake values were found in tumor and muscle for both radiolabeled αHER2 Fabs using quantitative image analysis (Table 2). Uptake values for liver and kidney from the PET measurements roughly match those from the biodistribution study. Apparent muscle activities were generally higher in the first instance, therefore leading to decreased tumor-to-muscle ratios.

**DISCUSSION**

Compared to conventional Fabs, which often suffer from premature kidney clearance, moderately prolonged plasma half-life leads to increased tumor uptake as well as tumor-to-blood ratio (*12*). PASylation, i.e. the fusion of a protein with a conformationally disordered amino acid polymer having PEG-like properties (*11*) can lead to improved tumor accumulation both due to the longer persistence in plasma and contact time and to the enhanced permeability and retention (EPR) effect (*23*). Contrasting with polyethylene glycol (PEG), the genetically encoded and biodegradable PAS tag requires no chemical modification and allows exact tuning of the

desired plasma half-life. Using the radio-iodinated protein tracer, we have demonstrated before that an approximately four-fold prolonged plasma half-life of 5.2 h compared with the unmodified αHER2 Fab, as realized by fusion with a PAS polypeptide of 200 amino acid residues (*11*), leads to favorable imaging contrast as well as tumor uptake (*12*).

Specific binding of this tailored Fab, labeled either with $^{124/125}$I or with $^{89}$Zr, to HER2-positive xenograft tumor was here verified in vivo by blocking experiments with the full size antibody Trastuzumab. Both PET and biodistribution analyses showed no unfavorable accumulation in most normal tissues, thus indicating stable radiolabeling and also confirming that modification with the biochemically inert PAS tag is compatible with in vivo imaging. In fact, PET imaging showed remarkably clear tumor imaging contrast 24 h p.i. Furthermore, excellent tumor-to-blood and tumor-to-normal tissue ratios were observed in dual-tracer in vivo biodistribution experiments.

Non-tumor related tracer accumulation was observed for the $^{89}$Zr-labeled Fab in kidney, liver and spleen and for the $^{124/125}$I-labeled Fab in thyroid. This distinct label-specific behavior can be explained by in vivo demetalation or deiodination, respectively. Moreover, the kidney uptake of $^{89}$Zr•Df-Fab-PAS$_{200}$ indicates that, despite an apparent molecular size above the threshold of the glomerular pores (*11*), the PASylated Fab is still excreted via renal filtration. Most likely, the protein tracer subsequently gets reabsorbed in proximal tubular cells, possibly via the endocytotic, ligand-specific receptors megalin or cubulin or via general pinocytosis (*24*). Following internalization, the labeled Fab is lysosomally catabolized into amino acids, which are released into the cytoplasm and returned into circulation, whereas Zr•Df-lysine/peptide conjugates (or the naked metal ion) remain trapped intracellularly. Conversely, iodotyrosine, the degradation product of a radio-iodinated protein, gets quickly released from cells after

endocytosis (by tumor cells, in the kidney or other tissues) (*25*), thus allowing redistribution in the body.

Notably, pronounced kidney accumulation has not been observed for $^{89}$Zr-labeled full size antibodies, probably owing to their extremely large molecular size and preferential clearance via the liver (*7, 10*), but was described for the $^{111}$In•DOTA-conjugated αHER2 Fab (*26*). Compared with the $^{89}$Zr-labeled Fab, other small protein tracers labeled with radiometals, e.g. the $^{111}$In-labeled αHER2 affibody DOTA-$Z_{HER2:342-pep2}$, have show even higher kidney uptake of >200 %ID/g 24 h p.i. – even though the participation of megalin/cubulin receptors in specific cellular uptake was excluded (*27*). On the other hand, the kidney uptake of (in terms of molecular size) the more closely related bivalent protein tracer $^{111}$In•DOTA-F(ab′)$_2$-Herceptin, with ~65 % ID/g 24 h p.i. (*28*), was in the same range as the one seen for our monovalent PASylated $^{89}$Zr-labeled Fab.

To offer guidance when choosing a suitable radiolabel in the preparation of protein tracers for clinical applications, we compared the two different radionuclides for the labeling of αHER2 Fab-$PAS_{200}$ side by side. Direct modification of the Fab with $^{124/125}$I is a fast and easy process, which did not affect target affinity, benefitting from the fact that Fabs contain several accessible tyrosine residues remote from their antigen-binding site. Similar functional results were obtained in case of the radiometal $^{89}$Zr while conjugation with the chelator derivative Df-SCN to free lysine side chains of the Fab was necessary prior to the actual radiolabeling. Nevertheless, this modification could be performed under mild conditions as well, thus preserving protein integrity and target affinity. As the protein portion of both (PASylated) $^{89}$Zr- and $^{124/125}$I-labeled Fabs was exactly identical, similar behavior in vivo could be expected. Hence, differences in the relative signals for tumor and organs such as kidney and liver should be caused by different routes of biochemical metabolization for the two radionuclides. To this end, we purposely did not apply

blocking reagents with regard to thyroid or kidney uptake (e.g. Lugol's solution, Irenat or Gelofusine (*24*)) – as it might be useful for clinical investigations – thus allowing unbiased comparison of tracer biodistribution.

In mouse PET experiments, the $^{124}$I-labeled Fab showed relatively fast blood clearance and high tumor-to-normal tissue ratio 24 h p.i., in line with the nature of $^{124}$I as a non-residualizing radionuclide. Free iodide, which occurs after intra- or extracellular dehalogenation in blood plasma, rapidly accumulates in the thyroid due to specific import via the sodium iodide symporter (*17*). In comparison, $^{89}$Zr•Df-Fab-PAS$_{200}$ showed slightly longer apparent life-time in circulation, which could indicate higher tracer stability. Remarkably, for this label almost five-fold higher tumor uptake was observed in the biodistribution analysis 24 h p.i., probably owing to the fact that $^{89}$Zr•Df is trapped inside the tumor cells after antigen binding and receptor-mediated internalization. Yet, despite slightly differing pharmacokinetic behavior of the two tracers, both essentially showed equally high tumor-to-blood ratio and good PET imaging contrast 24 h p.i.

Our observations are in line with results from previous investigations on the differences between residualizing and non-residualizing radiolabels. For example, a study utilizing different anti-carcinoembryonic antigen (CEA) single-chain Fv-Fc fusion proteins that were labeled either with $^{111}$In or $^{125}$I revealed higher tumor uptake of the radiometal (*29*). Furthermore, experiments with the head and neck squamous cell carcinoma-selective chimeric antibody U36, labeled either with $^{89}$Zr or with $^{124}$I, resulted in significantly higher uptake levels in tumor and liver for $^{89}$Zr (*30*). In a similar comparison of the $^{89}$Zr- and $^{124}$I-labeled versions of the anti-prostate stem cell antigen (PSCA) minibody A11 in mice carrying PSCA-positive tumors, higher tumor uptake was again found for the residualizing label, whereas better imaging contrast was seen for the $^{124}$I-labeled minibody (*31*).

Beside biodistribution studies in mice (*20*), $^{89}$Zr-labeled Trastuzumab was already tested in human patients with metastatic breast cancer (*10*), thus demonstrating potential for the non-invasive monitoring of the HER2 status during cancer progression. Consequently, clinical application of a protein tracer based on the corresponding Fab fragment should not be too difficult to achieve. Compared to the $^{89}$Zr-labeled full size mAb, our PASylated Fab with its optimized plasma half-life offers the advantage of high contrast in immuno-PET imaging already 24 h p.i. Notably, maximal contrast for the $^{89}$Zr•Df-Bz-SCN-trastuzumab in mice with HER2-positive BT474M1 xenografts was only reached 96–144 h p.i. (*20*), which is most likely explained by its very long circulation in blood.

## CONCLUSION

Taken together, distinct in vivo distribution profiles of two differently labeled αHER2 Fab tracers with optimized plasma half-life were observed, depending on the chemistries of the radioisotopes used for radiolabeling. Both the $^{89}$Zr- and the $^{124}$I-labeled Fab-PAS$_{200}$ exhibit equally high tumor-to-blood ratio and show strong PET imaging contrast 24 h p.i. However, based on the superior in vivo stability of the $^{89}$Zr-label and significantly higher tumor uptake overall, $^{89}$Zr•Df-Fab-PAS$_{200}$ appears as a preferred tracer for translation into the clinic.

## ACKNOWLEDGMENTS

This work was supported by ERC Grant MUMI from the European Union and the Collaborative Research Centre SFB-824 of the Deutsche Forschungsgemeinschaft. The authors wish to thank Dr. Calogero D'Alessandria for advice in zirconium labeling and Sybille Reder, Markus Mittelhäuser and Marco Lehmann for performing the imaging measurements.

**REFERENCES**


**1.** Tai W, Mahato R, Cheng K. The role of HER2 in cancer therapy and targeted drug delivery. *J Control Release.* 2010;146:264-275.

**2.** McCabe KE, Wu AM. Positive progress in immunoPET – not just a coincidence. *Cancer Biother Radiopharm.* 2010;25:253-261.

**3.** Lear-Kaul KC, Yoon HR, Kleinschmidt-DeMasters BK, McGavran L, Singh M. Her-2/*neu* status in breast cancer metastases to the central nervous system. *Arch Pathol Lab Med.* 2003;127:1451-1457.

**4.** Börjesson PK, Jauw YW, de Bree R, et al. Radiation dosimetry of $^{89}$Zr-labeled chimeric monoclonal antibody U36 as used for immuno-PET in head and neck cancer patients. *J Nucl Med.* 2009;50:1828-1836.

**5.** Divgi CR, Pandit-Taskar N, Jungbluth AA, et al. Preoperative characterisation of clear-cell renal carcinoma using iodine-124-labelled antibody chimeric G250 ($^{124}$I-cG250) and PET in patients with renal masses: a phase I trial. *Lancet Oncol.* 2007;8:304-310.

**6.** Disselhorst JA, Brom M, Laverman P, et al. Image-quality assessment for several positron emitters using the NEMA NU 4-2008 standards in the Siemens Inveon small-animal PET scanner. *J Nucl Med.* 2010;51:610-617.

**7.** Meijs WE, Haisma HJ, Klok RP, et al. Zirconium-labeled monoclonal antibodies and their distribution in tumor-bearing nude mice. *J Nucl Med.* 1997;38:112-118.

**8.** Severin GW, Engle JW, Barnhart TE, Nickles RJ. $^{89}$Zr radiochemistry for positron emission tomography. *Med Chem.* 2011;7:389-394.

**9.** Perik PJ, Lub-De Hooge MN, Gietema JA, et al. Indium-111-labeled trastuzumab scintigraphy in patients with human epidermal growth factor receptor 2-positive metastatic breast cancer. *J Clin Oncol.* 2006;24:2276-2282.

**10.** Dijkers EC, Oude Munnink TH, Kosterink JG, et al. Biodistribution of $^{89}$Zr-trastuzumab and PET imaging of HER2-positive lesions in patients with metastatic breast cancer. *Clin Pharmacol Ther.* 2010;87:586-592.

**11.** Schlapschy M, Binder U, Börger C, et al. PASylation: a biological alternative to PEGylation for extending the plasma half-life of pharmaceutically active proteins. *Protein Eng Des Sel.* 2013;26:489-501.

**12.** Mendler CT, Friedrich L, Laitinen I, et al. High contrast tumor imaging with radio-labelled antibody Fab fragments tailored for optimized pharmacokinetics via PASylation. *mAbs.* 2015;7:96-109.

**13.** Holmes WE, Sliwkowski MX, Akita RW, et al. Identification of heregulin, a specific activator of p185$^{erbB2}$. *Science.* 1992;256:1205-1210.

**14.** Vosjan MJ, Perk LR, Visser GW, et al. Conjugation and radiolabeling of monoclonal antibodies with zirconium-89 for PET imaging using the bifunctional chelate p-isothiocyanatobenzyl-desferrioxamine. *Nat Protoc.* 2010;5:739-743.

**15.** Perk LR, Vosjan MJ, Visser GW, et al. *p*-Isothiocyanatobenzyl-desferrioxamine: a new bifunctional chelate for facile radiolabeling of monoclonal antibodies with zirconium-89 for immuno-PET imaging. *Eur J Nucl Med Mol Imaging.* 2010;37:250-259.

**16.** Behr TM, Goldenberg DM, Becker W. Reducing the renal uptake of radiolabeled antibody fragments and peptides for diagnosis and therapy: present status, future prospects and limitations. *Eur J Nucl Med.* 1998;25:201-212.

**17.** Darrouzet E, Lindenthal S, Marcellin D, Pellequer JL, Pourcher T. The sodium/iodide symporter: state of the art of its molecular characterization. *Biochim Biophys Acta.* 2014;1838:244-253.

**18.** Hosseinimehr SJ, Tolmachev V, Orlova A. Liver uptake of radiolabeled targeting proteins and peptides: considerations for targeting peptide conjugate design. *Drug Discov Today.* 2012;17:1224-1232.

**19.** Dijkers EC, Kosterink JG, Rademaker AP, et al. Development and characterization of clinical-grade $^{89}$Zr-trastuzumab for HER2/*neu* immunoPET imaging. *J Nucl Med.* 2009;50:974-981.

**20.** Tinianow JN, Gill HS, Ogasawara A, et al. Site-specifically $^{89}$Zr-labeled monoclonal antibodies for ImmunoPET. *Nucl Med Biol.* 2010;37:289-297.

**21.** Duncan JR, Behr TM, DeNardo SJ. Intracellular fate of radiometals. *J Nucl Med.* 1997;38:829.

**22.** Boswell CA, Marik J, Elowson MJ, et al. Enhanced tumor retention of a radiohalogen label for site-specific modification of antibodies. *J Med Chem.* 2013;56:9418-9426.

**23.** Gao W, Liu W, Christensen T, Zalutsky MR, Chilkoti A. In situ growth of a PEG-like polymer from the C terminus of an intein fusion protein improves pharmacokinetics and tumor accumulation. *Proc Natl Acad Sci U S A.* 2010;107:16432-16437.

**24.** Vegt E, de Jong M, Wetzels JF, et al. Renal toxicity of radiolabeled peptides and antibody fragments: mechanisms, impact on radionuclide therapy, and strategies for prevention. *J Nucl Med.* 2010;51:1049-1058.

**25.** Shih LB, Thorpe SR, Griffiths GL, et al. The processing and fate of antibodies and their radiolabels bound to the surface of tumor cells in vitro: a comparison of nine radiolabels. *J Nucl Med.* 1994;35:899-908.

**26.** Dennis MS, Jin H, Dugger D, et al. Imaging tumors with an albumin-binding Fab, a novel tumor-targeting agent. *Cancer Res.* 2007;67:254-261.

**27.** Altai M, Varasteh Z, Andersson K, Eek A, Boerman O, Orlova A. *In vivo* and *in vitro* studies on renal uptake of radiolabeled affibody molecules for imaging of HER2 expression in tumors. *Cancer Biother Radiopharm.* 2013;28:187-195.

**28.** Smith-Jones PM, Solit DB, Akhurst T, Afroze F, Rosen N, Larson SM. Imaging the pharmacodynamics of HER2 degradation in response to Hsp90 inhibitors. *Nat Biotechnol.* 2004;22:701-706.

**29.** Kenanova V, Olafsen T, Williams LE, et al. Radioiodinated versus radiometal-labeled anti-carcinoembryonic antigen single-chain Fv-Fc antibody fragments: optimal pharmacokinetics for therapy. *Cancer Res.* 2007;67:718-726.

**30.** Verel I, Visser GW, Boerman OC, et al. Long-lived positron emitters zirconium-89 and iodine-124 for scouting of therapeutic radioimmunoconjugates with PET. *Cancer Biother Radiopharm.* 2003;18:655-661.

**31.** Knowles SM, Zettlitz KA, Tavaré R, et al. Quantitative immunoPET of prostate cancer xenografts with $^{89}$Zr- and $^{124}$I-labeled anti-PSCA A11 minibody. *J Nucl Med.* 2014;55:452-459.

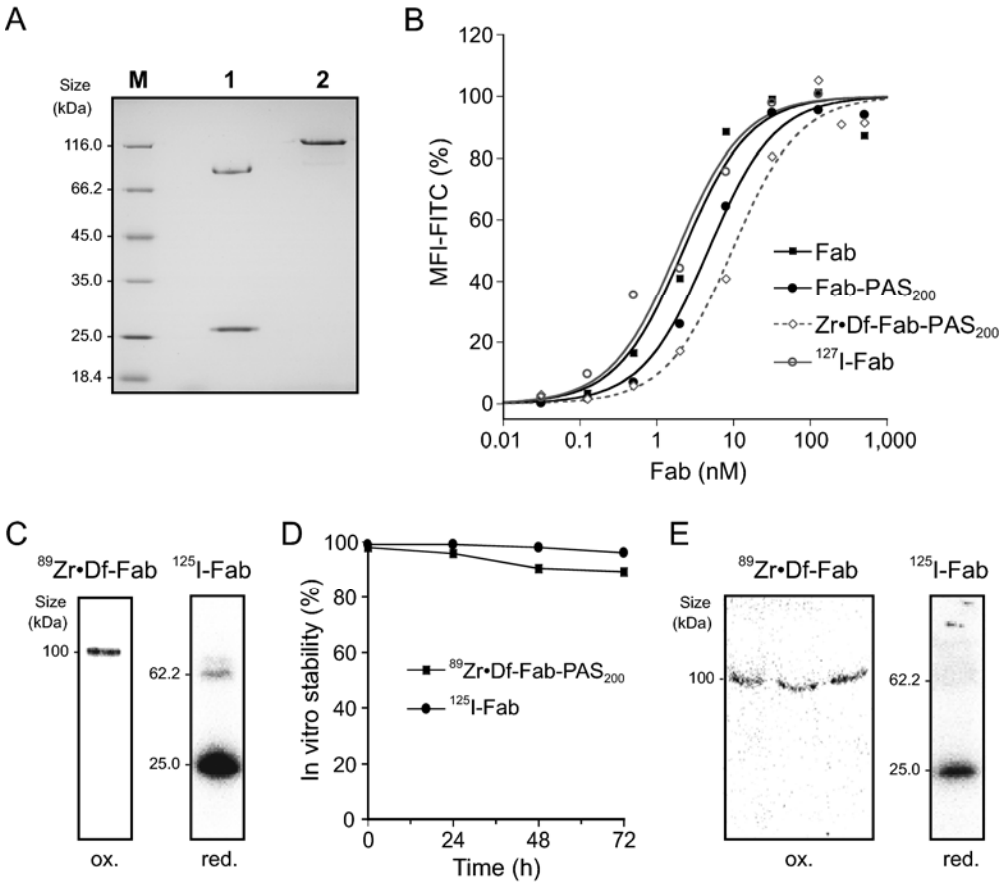


**Fig. 1. Characterization of purified Fab-PAS$_{200}$. (A)** SDS-PAGE of purified Fab-PAS$_{200}$ under reducing (lane 1) and non-reducing (lane 2) conditions. M, molecular size marker. **(B)** FACS titration analysis on HER2-positive cells of modified Fabs in different formats. $K_D$ values of 2.2 ± 0.6 nM for the unmodified Fab, 4.7 ± 0.7 nM for Fab-PAS$_{200}$, 1.8 ± 0.5 for the iodinated Fab (data taken from (*12*)) and 9.6 ± 2.0 nM for $^{90\text{-}94}$Zr•Df-Fab-PAS$_{200}$ were determined. **(C)** SDS-PAGE of radiolabeled $^{89}$Zr•Df-Fab-PAS$_{200}$ under non-reducing conditions as well as $^{125}$I-Fab-PAS$_{200}$ under reducing conditions. Radioactivity was detected via phosphorimager analysis. **(D)** In vitro stability of $^{89}$Zr•Df-Fab-PAS$_{200}$ and $^{125}$I-Fab-PAS$_{200}$ in PBS was analyzed at various time points up to 72 h by quantifying protein-associated radioactivity via SEC and TLC. **(E)** Serum samples of tumor bearing mice injected with $^{89}$Zr•Df-Fab-PAS$_{200}$ or $^{125}$I-Fab were analyzed 24 h p.i. after SDS-PAGE on a phosphorimager.

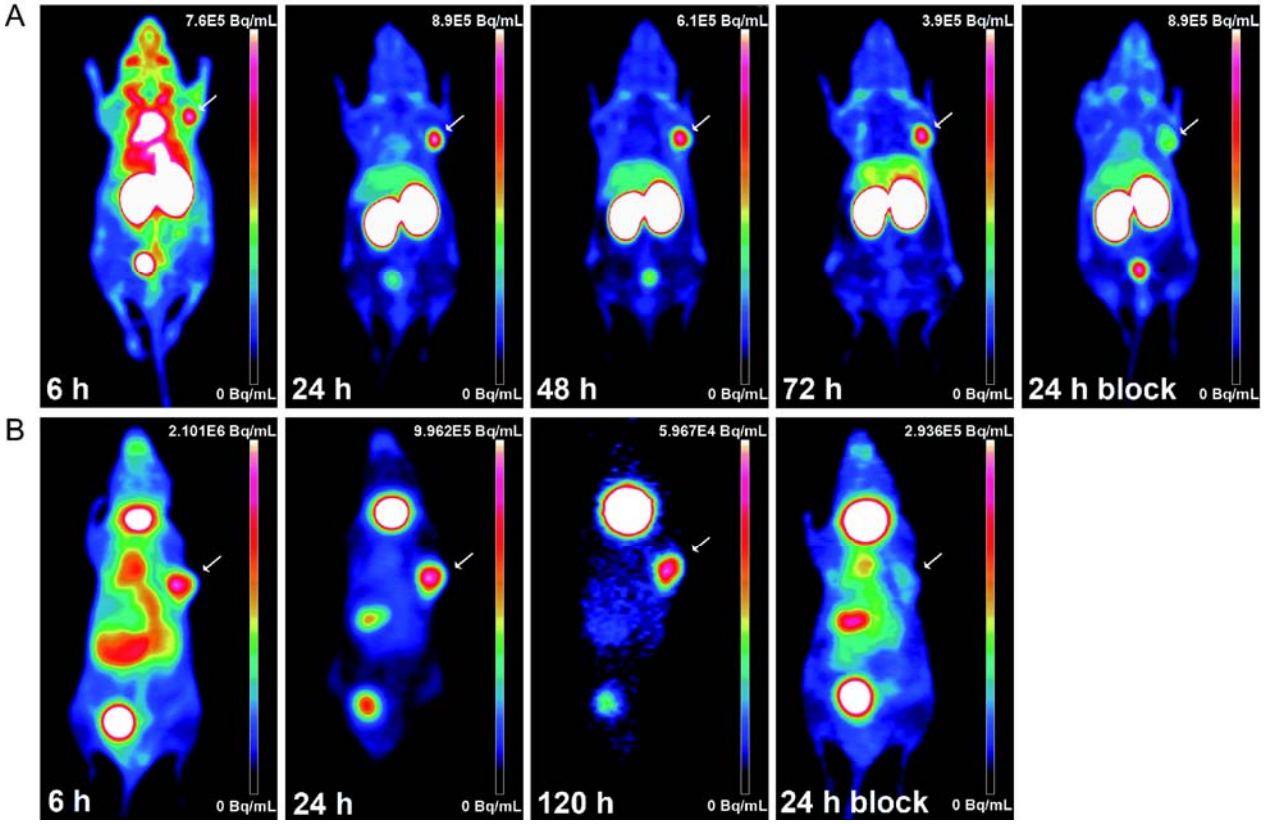


**Fig. 2. MIP-PET images of xenograft tumors in mice using $^{89}$Zr- and $^{124}$I-labeled αHER2 Fab-PAS$_{200}$.** CD1-*Foxn1*$^{nu}$ mice bearing s.c. HER2-positive (SK-BR-3) human tumor xenografts in the right shoulder (arrow) were injected i.v. with 7 MBq $^{89}$Zr- or $^{124}$I-labelled Fab-PAS$_{200}$. PET scans were performed for **(A)** $^{89}$Zr•Df-Fab-PAS$_{200}$ and **(B)** $^{124}$I-Fab-PAS$_{200}$ (data taken from (*12*)).

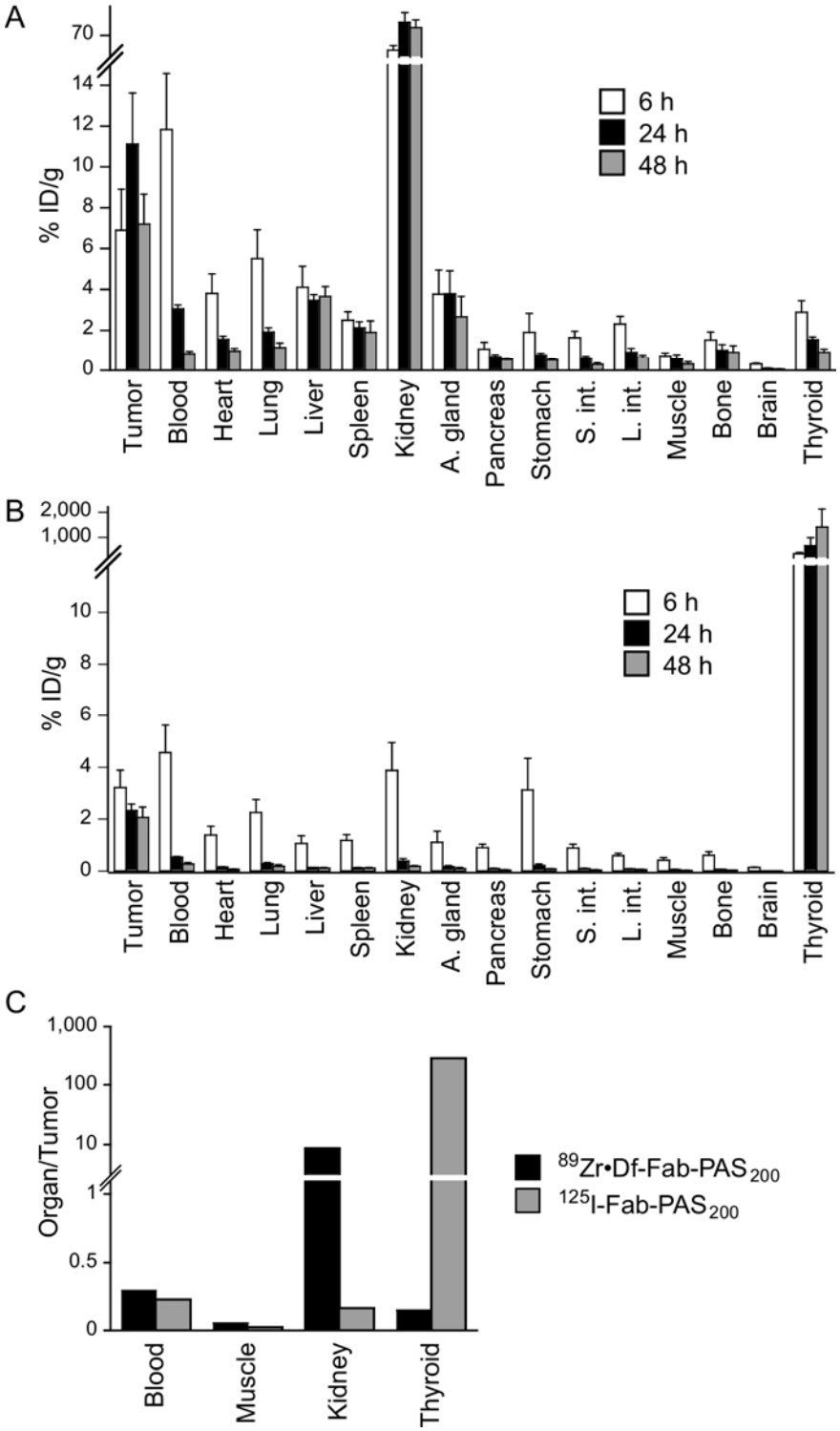


**Fig. 3: Dual tracer biodistribution analysis of $^{89}$Zr- and $^{125}$I-labeled αHER2 Fab-PAS$_{200}$.** Biodistribution of the two radiolabeled Fabs, injected simultaneously, was investigated 6 h (white bars), 24 h (black bars) and 48 h (grey bars) p.i. The percentage of injected dose per gram (%

ID/g) for all analyzed organs is plotted for **(A)** $^{89}$Zr•Df-Fab-PAS$_{200}$ and **(B)** $^{125}$I-Fab-PAS$_{200}$ (mean values ± standard deviation; n=5). **(C)** Direct comparison of relevant organ-to-tumor ratios 24 h p.i. between $^{125}$I- and $^{89}$Zr-labeled αHER2 Fab-PAS$_{200}$ (mean values; n=5).

## TABLES

**Table 1:** Biodistribution of $^{125}$I- and $^{89}$Zr-labeled αHER2 Fab-PAS$_{200}$

| | $^{89}$Zr•Df-Fab-PAS$_{200}$ | | | | $^{125}$I-Fab-PAS$_{200}$ | | | |
|---|---|---|---|---|---|---|---|---|
| **[%ID/g]** | **6 h** | **24 h** | **Block (24 h)** | **48 h** | **6 h** | **24 h** | **Block (24 h)** | **48 h** |
| Tumor | 6.89±2.02 | 11.11±1.73 | 3.11±0.35 | 7.19±1.46 | 3.21±0.68 | 2.33±0.25 | 0.33±0.06 | 2.06±0.40 |
| Blood | 11.84±2.73 | 3.05±0.19 | 2.55±0.53 | 0.82±0.13 | 4.56±1.06 | 0.53±0.04 | 0.52±0.10 | 0.27±0.05 |
| Heart | 3.79±0.97 | 1.55±0.15 | 1.40±0.39 | 0.96±0.14 | 1.38±0.34 | 0.15±0.01 | 0.16±0.05 | 0.07±0.01 |
| Lung | 5.50±1.41 | 1.90±0.20 | 1.58±0.31 | 1.13±0.23 | 2.25±0.50 | 0.28±0.04 | 0.28±0.05 | 0.18±0.05 |
| Liver | 4.11±1.03 | 3.45±0.29 | 2.96±0.69 | 3.65±0.48 | 1.06±0.29 | 0.13±0.01 | 0.12±0.02 | 0.11±0.02 |
| Spleen | 2.48±0.41 | 2.10±0.30 | 1.36±0.78 | 1.88±0.56 | 1.18±0.22 | 0.12±0.01 | 0.14±0.02 | 0.10±0.03 |
| Kidney | 49.4±6.6 | 88.3±12.8 | 70.7±14.3 | 80.7±10.4 | 3.87±1.07 | 0.38±0.09 | 0.34±0.06 | 0.18±0.03 |
| A. gland | 3.76±1.18 | 3.77±1.12 | 2.26±0.28 | 2.65±0.99 | 1.11±0.43 | 0.17±0.03 | 0.16±0.03 | 0.09±0.04 |
| Pancreas | 1.06±0.32 | 0.68±0.09 | 0.63±0.18 | 0.52±0.09 | 0.90±0.13 | 0.09±0.01 | 0.11±0.04 | 0.04±0.01 |
| Stomach | 1.87±0.95 | 0.76±0.09 | 0.62±0.15 | 0.51±0.05 | 3.12±1.22 | 0.21±0.06 | 0.28±0.18 | 0.08±0.01 |
| S. int. | 1.61±0.32 | 0.62±0.08 | 0.63±0.17 | 0.29±0.07 | 0.89±0.14 | 0.09±0.01 | 0.10±0.02 | 0.04±0.01 |
| L. int. | 2.28±0.38 | 0.91±0.18 | 0.88±0.24 | 0.62±0.13 | 0.59±0.09 | 0.08±0.02 | 0.09±0.03 | 0.05±0.01 |
| Muscle | 0.72±0.16 | 0.55±0.23 | 0.47±0.09 | 0.30±0.11 | 0.41±0.11 | 0.05±0.02 | 0.06±0.00 | 0.02±0.01 |
| Bone | 1.52±0.38 | 1.01±0.27 | 0.84±0.20 | 0.91±0.32 | 0.61±0.13 | 0.06±0.01 | 0.07±0.01 | 0.03±0.01 |
| Brain | 0.30±0.05 | 0.09±0.01 | 0.07±0.01 | 0.04±0.01 | 0.13±0.02 | 0.01±0.00 | 0.01±0.00 | 0.01±0.00 |
| Thyroid | 2.88±0.55 | 1.52±0.14 | 1.03±0.33 | 0.90±0.17 | 366±49 | 673±318 | 461±138 | 1412±710 |
| T/Blood | 0.6 | 3.6 | 1.2 | 8.8 | 0.7 | 4.4 | 0.6 | 7.8 |
| T/Muscle | 9.6 | 20 | 6.7 | 24 | 7.8 | 43 | 5.3 | 101 |

**Table 2:** Quantitation of PET images (n=1–2) for $^{125}$I- and $^{89}$Zr-labeled αHER2 Fab-PAS$_{200}$

| | **$^{89}$Zr•Df-Fab-PAS$_{200}$** | | | | **$^{125}$I-Fab-PAS$_{200}$** | | |
|---|---|---|---|---|---|---|---|
| **[%ID/g]** | **6 h** | **24 h** | **48 h** | **72 h** | **6 h** | **24 h** | **120 h** |
| Tumor | 10 | 13 | 10 | 6.2 | 6.8 | 2.4 | 0.4 |
| Muscle | 1.7 | 0.8 | 0.9 | 0.6 | 0.7 | 0.2 | 0.004 |
| Liver | 9.4 | 7.6 | 5.1 | 3.7 | 3.7 | 1.5 | 0.1 |
| Kidney | 62 | 62 | 56 | 34 | 3.4 | 0.9 | 0.03 |
| T/Muscle | 6.2 | 17 | 11 | 9.8 | 9.7 | 15.7 | 85 |